Journal of Electron Microscopy **58(3)**: 137–145 (2009)
doi: 10.1093/jmicro/dfp006

Special number: Instrumentation/Performance

Phase TEM for biological imaging utilizing a Boersch electrostatic phase plate: theory and practice

Jessie Shiue[1], Chia-Seng Chang[1], Sen-Hui Huang[4], Chih-Hao Hsu[4], Jin-Sheng Tsai[3], Wei-Hau Chang[2], Yi-Min Wu[2], Yen-Chen Lin[2], Pai-Chia Kuo[1], Yang-Shan Huang[1], Yeukuang Hwu[1,3], Ji-Jung Kai[4], Fan-Gang Tseng[4] and Fu-Rong Chen[1,3,4,*]

[1]Institute of Physics, [2]Institute of Chemistry, Academia Sinica, Nankang 11529, Taipei, [3]National Synchrotron Radiation Research Center, HsinChu 30076 and [4]Department of Engineering and System Science, National TsingHua University, HsinChu 30043, Taiwan
*To whom correspondence should be addressed. E-mail: frchen@ess.nthu.edu.tw

Abstract A Boersch electrostatic phase plate (BEPP) used in a transmission electron microscope (TEM) system can provide tuneable phase shifts and overcome the low contrast problem for biological imaging. Theoretically, a pure phase image with a high phase contrast can be obtained using a BEPP. However, a currently available TEM system utilizing a BEPP cannot achieve sufficiently high phase efficiency for biological imaging, owing to the practical conditions. The low phase efficiency is a result of the blocking of partial unscattered electrons by BEPP, and the contribution of absorption contrast. The fraction of blocked unscattered beam is related to BEPP dimensions and to divergence of the illumination system of the TEM. These practical issues are discussed in this paper. Phase images of biological samples (negatively stained ferritin) obtained by utilizing a BEPP are reported, and the phase contrast was found to be enhanced by a factor of ~1.5, based on the calculation using the Rose contrast criterion. The low gain in phase contrast is consistent with the expectation from the current TEM/BEPP system. A new generation of phase TEM utilizing BEPP and designed for biological imaging with a high phase efficiency is proposed.

Keywords phase TEM, Beorsch phase plate, Zernike phase plate, electrostatic phase plate, biological imaging, phase contrast

Received 2 December 2008, accepted 20 January 2009, online 16 March 2009

Introduction

One of the bottlenecks for biological imaging in a transmission electron microscope (TEM) is low contrast due to the weak interactions of the incident beam with materials composed of light elements. Development of electron phase plates to construct a phase contrast TEM in analogy with a phase contrast optical microscope has become an urgent research topic for biological imaging. Nagayama and Danev have successfully demonstrated the contrast improvement with the Zernike phase plate made of carbon film [1–3]. However, the phase shift provided by this thin-film-type phase plate cannot be tuned and its application is hence limited. Alternatively, a Boersch electrostatic phase plate (BEPP) (also called Zernike electrostatic phase plate, ZEPP) would have more benefits. Originally proposed by Boersch [3], and later discussed by Matsumoto and Tonomura [4], BEPPs can provide tuneable phase shifts, and have been explored intensively in recent years [5–8]. The figure of merit for a tuneable phase plate is not only that the phase contrast images can be recorded, but also that the complete exit wave can possibly be reconstructed.

Another obstacle in biological imaging is the radiation damage to the samples, and low-dose image technique is therefore needed for imaging some biological samples. The TEM instrument equipped with Zernike phase plate in terms of low-dose imaging performance has been evaluated by

Malac *et al*. [8]. It has been shown that a TEM equipped with a Zernike phase plate (or BEPP) to vary the phase plate thickness (for example, by changing the electrostatic bias of the phase plate) can benefit low-dose microscopy for application of biological samples [8].

The original proposed geometry of BEPP is a ring supported with a straight cantilever [4]. The BEPP has a five-layered structure that builds an electrostatic field in the center of the ring to modify the phase shift of the incident electron beam [4]. The amount of phase shift is controlled by the voltage applied to the two outer electrodes. For biological imaging in a TEM utilizing a BEPP, however, many theoretical and practical issues would need to be considered. This paper aims at discussing these issues and provides an overall consideration of a phase TEM equipped with a BEPP for biological imaging with high efficiency of transfer of object phase into image contrast. The biological samples of negatively stained ferritin were used in this work for comparing the results obtained by using our BEPP and by using a carbon-film-type phase plate, which was achieved by Danev and Nagayama [1]. Furthermore, Fe in the core of ferritin may contribute to the expected 'absorption' contrast, and thus can be used to demonstrate the mixed contrast of 'absorption' and 'phase' contrast from BEPP. The mixture of the two contrasts will be discussed.

In this paper, the following is reported. First, we provide a brief contrast theory for weak objects in order to understand the differences between the theoretical and the practical conditions. Second, a suitable design of a BEPP for biological imaging is presented, and the background of such a design is discussed. Third, we report on the first successful case of phase TEM images of biological samples (negatively stained ferritin) obtained by using a BEPP, and study its gain of phase contrast and phase efficiency. Finally, an effective phase TEM design utilizing a BEPP for biological imaging is suggested.

Design of a Boersch electrostatic phase plate for biological imaging

Among the reported work on fabrication of BEPPs [5–7], phase contrast enhancement has only been successfully presented by Huang *et al*. on a bi-layer structure of amorphous SiO_2 and $SiON_x$ [5]. However, the observed gain of contrast was much lower than the theoretical expectation, due to the contribution of absorption contrast as suggested in their report.

In reality, a phase plate provides not only the phase contrast in an image, but also a mixture of 'phase' contrast and 'absorption' contrast [9]. Two types of contrast are involved in imaging in a TEM: (i) amplitude contrast (or 'absorption' contrast), which is accomplished by preventing some of the scattered electron from reaching the image plane and (ii) phase contrast, which is accomplished by introducing a path difference between the scattered and unscattered waves before allowing them to interfere. These two types of contrast would both need to be taken into consideration while designing a BEPP for biological imaging. It is favorable for the BEPP to enhance the phase contrast but lower the absorption contrast.

(a) Simplified theory of phase contrast and absorption contrast associated with a Boersch electrostatic phase plate

A brief review of contrast theory for weak objects (with light elements) is given here in order to understand the differences between the theoretical and the practical situations of a TEM system with a BEPP. Although there are some theoretical discussions and calculations of phase contrast with phase plates [1,10], the rather simplified theory is only applicable to very thin objects composed of light elements. It was noted that both carbon-film-based [1,10] and Boersch-type [9] phase plates reduce the number of electrons available for coherent phase imaging. This effect may give rise to 'absorption' contrast, and is discussed in our previous report [9].

In the case of a light and thin object, the exit wave can be approximated [11]:

$$\psi_e = \exp[-\sigma V'(r)t]\exp[i\sigma V\ (r)t] \cong 1 - \sigma V'(r)t + i\sigma V\ (r)t \tag{1}$$

where the first term represents the object which is illuminated with a uniform and parallel source, $V(r)$ is the real potential which is responsible for the phase change and $V'(r)$ is the imaginary part of potential, responsible for the 'absorption'; σ is the interaction constant where $\sigma = 2\pi\lambda m/h^2$, t is the thickness of the thin slice, λ is the wavelength of the incident electron and m is the mass of the electron. The $V(r)$ and $V'(r)$ terms have Fourier components of V_g and V'_g, respectively.

V_o and V_o' give the mean values of the real potential $V(r)$ and the imaginary potential $V'(r)$, which are related to the mean refractivity and absorption of the thin slice, respectively [9]. In the back focal plane, the electron wave is

$$\begin{aligned}\psi_d &= \Im(\psi_e) = \delta - \Im(\sigma V'(r)t) + i\Im(\sigma V\ (r)t)\\ &= [\delta - \sigma V_o' t + i\sigma V_o t]_{g=0} - \sigma t\sum_{g\neq 0} V_g' + i\sigma t\sum_{g\neq 0} V_g. \end{aligned}\tag{2}$$

An unscattered beam produces a very sharp spot under a perfectly parallel and uniform illumination incident electron beam. As the electron beam passes through the lens, the intensity of the bright-field image, $I(r)$, is determined by the interference between the unscattered wave ($g = 0$) and the higher order scattered wave ($g \neq 0$) that is phase shifted by the lens aberration:

$$\begin{aligned}I(r) &= 1 - 2\sigma V'(r)t \otimes \Im[A(g)\cos\chi(g)] + 2\sigma V(r)t\\ &\otimes\Im[A(g)\sin\chi(g)]\end{aligned}\tag{3}$$

where $\otimes$ indicates the operation of convolution, $A(g)$ is the virtual aperture and $\chi(g)$ is the lens aberration function contributed by spherical aberration and defocus. The first,

second and third terms represent the uniform background, the 'absorption' image and the phase image, respectively. If the size of a phase plate can be made to be infinitely small so as to alter only the phase of the central unscattered wave ($g = 0$) by $\pi/2$ in Eq. (2), the image intensity would become

$$I(r) = 1 - 2\sigma V(r)t \otimes \Im[A(g)\cos\chi(g)] + 2\sigma V'(r)t \otimes \Im[A(g)\sin\chi(g)]. \quad (4)$$

Most biological microscopy is limited to a resolution far poorer than 1 nm due to radiation damage and staining effects. Within this resolution ($g < 1$ nm^{-1}), the lens aberration (C_s) may be ignored. For the application of a phase plate, the object is imaged at a Gaussian focus ($\Delta f \sim 0$), i.e. $\cos\chi \sim 1$ and $\sin\chi \sim 0$. Equations (3) and (4) can therefore be simplified to Eqs (5) and (6), respectively:

$$I(r) = 1 - 2\sigma V'(r)t \otimes \Im[A(g)] \quad (5)$$

$$I(r) = 1 - 2\sigma V(r)t \otimes \Im[A(g)]. \quad (6)$$

Equation (5) is a pure 'absorption' image, which predicts an image showing dark contrast in regions of large 'mass thickness', while Eq. (6) is a pure phase contrast image, which reflects the projected potential of the sample. Similar to the absorption image, the phase contrast image shows dark contrast in regions of high potential. In general, the real part of the potential $V(r)$ is about 10 times larger than the imaginary part of the potential $V'(r)$ [9,12–15]. Therefore, roughly 10 times contrast enhancement is expected in a perfect system utilizing a perfect phase plate.

It should be noted, however, that the equations derived above are valid only under the following assumptions:

(i) The BEPP is a two-dimensional device, and is infinitely small, so that only the phases of unscattered beams are altered by the electrostatic field produced by the phase plate.

(ii) The phase plate does not exclude any components of the exit wave given in Eq. (2), and 100% of transmission beams pass through the central hole of the phase plate.

(iii) The incident beams are perfectly coherent, parallel and form a uniform illumination source, so that the unscattered beams localize to become a very sharp spot at the center of the back focal plane.

These assumptions, however, do not correspond to the real conditions of a currently available TEM system adopting a BEPP. Here are the facts:

(b) Practical issues concerning the Boersch electrostatic phase plate

The rule of cut-off frequency

Practically, the size of the phase plate cannot be made to be infinitely small. Therefore, not only the unscattered beams are phase shifted, but partial scattered beams in the low-frequency range may also enter the central hole of the phase plate, be phase shifted and complicate the phase contrast image. It has been proposed that the phase contrast may depend on the cut-off frequency, g_c, of the phase plate which is reciprocally proportional to the size of object [1]. To see a noticeable phase contrast, the rule of cut-off frequency requires that the size of object, S, must be smaller than $1/g_c$. The cut-off frequency is determined by

$$g_c = \frac{r}{\lambda f} \quad (7)$$

where r represents the distance from the center to the edge of the phase plate, λ is the electron wavelength and f is the focal length.

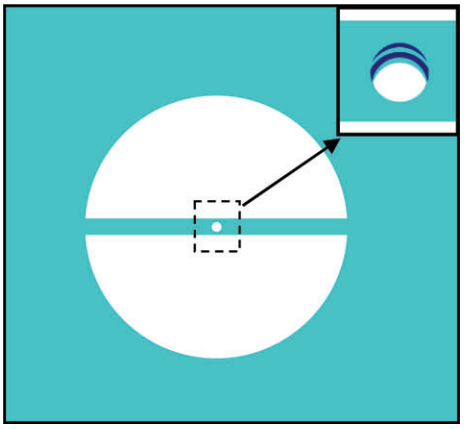

Fig. 1. Schematic of a new Boersch electrostatic phase plate (BEPP) design: a long straight narrow cantilever (<80 μm in length) with a fiver-layered structure, which has a small central hole in the middle of the cantilever. The inset shows the tilted view of the central hole (with diameter <1 μm) where the five-layered structure is revealed: the insulating layers are demonstrated in dark blue, and the metal layers are shown in light blue.

As shown in Fig. 1, a new and simple design of a BEPP is reported here. Compared with the conventional ring design of a BEPP, our present phase plate design is a straight narrow cantilever with a width of ~2.0 μm, which has a small central hole with a diameter of ~0.8 μm. In this work, the TEM had a focal length of 2.7 mm and was operated at 100 keV and r was 1.0 μm (half width of the cantilever), giving the cut-off frequency in this work:

$$g_c = \frac{r}{\lambda f} = \frac{1 \times 10^{-6}}{(0.037 \times 10^{-10}) \times (2.7 \times 10^{-3})} = 0.1 \text{ nm}^{-1}.$$

The reciprocal of g_c is 10 nm, which corresponds to the upper limit of the sample size to be imaged. It has roughly the same dimension as the objects (negatively stain ferritin) studied in this work.

Equation (7) suggests that the size of the phase plate (r) shall be as small as possible in order to be workable for large objects. Nevertheless, the size of the phase plate cannot be infinitely small due to some practical problems. These problems are discussed in the following.

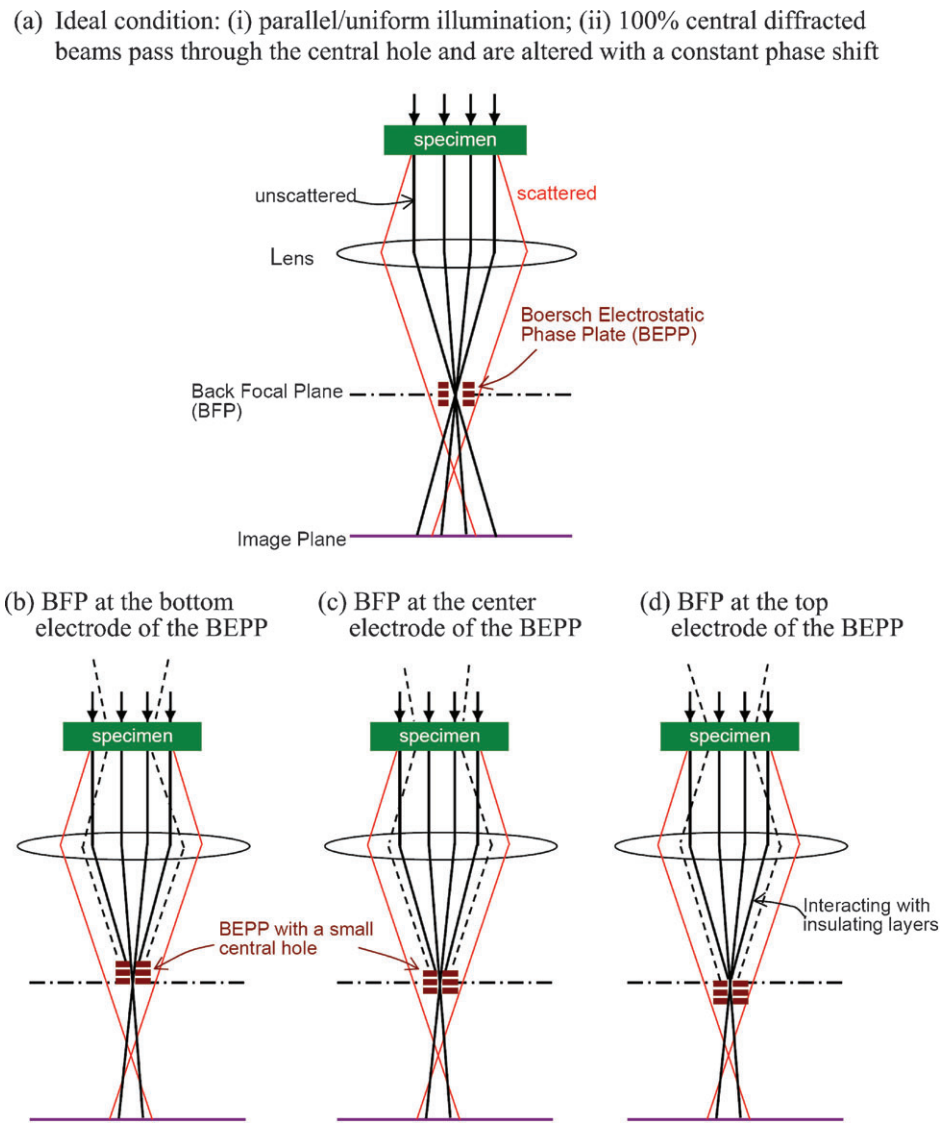

Fig. 2. Optical geometry and the location of the phase plate in a TEM system. The black solid lines represent the electron beam from parallel illumination; the dashed lines represent the electron beams from Gaussian illumination (beam divergence). The red lines represent the scattered electron beams. (a) The ideal system with a parallel/uniform illumination in which all the central diffracted beams pass through the central hole of the phase plate and are altered with a constant phase shift; (b) the back focal plane is located at the bottom electrode of the phase plate with a small central hole and partial unscattered beams are blocked by the phase plate; (c) the back focal plane is located at the central electrode of the phase plate with a small central hole and partial unscattered beams are blocked by the phase plate; (d) the back focal plane is located at the top electrode of the phase plate with a small central hole and partial unscattered beams interact with the insulating layers and cause charging effect.

Reduction in the efficiency of the phase contrast

The phase contrast theory for the phase plate always assumes that the sample is illuminated with parallel and uniform electron beams which lead transmission (unscattered) beams to become a sharp delta point in the back focal plane, as described in Eq. (2). Under these perfect conditions, the central diffracted beams completely fall inside the central hole of the BEPP, and are altered with a constant phase shift, as schematically shown in Fig. 2a.

In a real system, however, the condition is not as perfect as the one demonstrated in Fig. 2a, and there are several practical situations making the condition of Eq. (2) invalid.

1. Geometry of a BEPP

A BEPP is not a two-dimensional device, but rather a three-dimensional one. The height of our phase plate is ~1.4 μm. In our present system set-up, the *z*-height of the BEPP can be controlled by a piezo-driver. The relative positions of the BEPP and the focal plane are controlled by the combination of condenser/objective lenses and the piezo-driver.

Figure 2b, c and d show that the back focal plane is located at the bottom electrode, the central electrode and the top electrode of the BEPP, respectively. The traces of electron beams for parallel illumination are given as solid lines in these figures. As the size of the central hole of the BEPP is reduced, only partial transmission beams are subjected to phase shift in the cases shown in Fig. 2b and c, where the unscattered beams are focused at the bottom and the central electrode, respectively. In the case shown in Fig. 2d, the unscattered electrons after the focal plane interacted with the insulating layers of the BEPP, causing charging effects and resulting in blurring of images.

Assuming that only a fraction, η, of unscattered electrons pass through the central hole of the phase plate, the pure phase image intensity in Eq. (6) would become

$$I(r) = \eta^2 - 2\eta\sigma V(r)t \otimes \Im[A(g)]. \tag{8}$$

The first term presents the uniform background and the second term gives the phase contrast. The phase contrast is reduced linearly by a fraction of η, where $\eta < 1$. In Eq. (8), the intensity of a uniform background is reduced by a factor of η^2 as compared with the case given in Eq. (6). The parameter η is related to the efficiency of the phase contrast. On reducing the dimension of the central hole of the phase plate, the exposure time would need to be increased to gain the phase signal against the noise. Equation (8) should be modified to include a noise term, Δ:

$$I(r) = \eta^2 - 2\eta\sigma V(r)t \otimes \Im[A(g)] + \Delta. \tag{9}$$

To an extreme, all the useful signals would be lost if the size of the phase plate is shrunk to delta point size.

2. Illumination: beam divergency

Practically, the electron beams may not be ideally parallel and form a uniform illumination source. The efficiency of the phase contrast is thus further worsened due to the effect of beam divergence. A reasonable assumption for the beam function $B(r)$ is a Gaussian. The exit wave shown in Eq. (1) therefore becomes

$$\psi_e \cong B(r)[1 - \sigma V'(r)t + i\sigma V(r)t]. \tag{10}$$

In the back focal plane, the electron wave would be

$$\psi_d(g) = \Im(B(r)) \otimes [\delta - \sigma\Im(V'(r))t + i\sigma\Im(V(r))t]. \tag{11}$$

In the back focal plane, both unscattered and scattered beams are broadened by the Fourier transform of $B(r)$, which is also a Gaussian. The broadening effect is larger for an LaB_6 electron gun (used in the JEOL 2000FX TEM for this work) compared to a field emission gun. The traces of electron beams for Gaussian illumination are given as dashed lines in Fig. 2b, c and d. As shown in these figures, the beam divergence effect that resulted from non-parallel illumination would further reduce the amounts of unscattered beams passing through the central hole of a BEPP.

Figure 3 shows a diffraction pattern recorded without any sample in the beam path. The exposure time was 0.5 s and the condenser lens aperture was the smallest (20 μm). Since there was no sample in the beam path, the diffraction spot mainly resulted from the unscattered beams. The phase plate was inserted as a calibration reference. The diameter of the central hole was 0.8 μm and the diameter of the unscattered beam was calibrated to be 1.5 μm. The fraction η of unscattered beams passing through the central hole was calculated to be ∼10% (0.1).

3. Mixing of phase and absorption contrast

Practically, the size of a phase plate cannot be infinitely small. The partial scattered beam was also prevented by the cantilever of the phase plate from forming an image. The image recorded using the BEPP contained a mixture of 'phase' and 'absorption' contrast. The image intensity can therefore be rewritten as

$$I(r) = \eta^2 - 2\sigma V'(r)t \otimes \Im[A(g)] - 2\eta\sigma V(r) \otimes \Im[A(g)]. \tag{12}$$

The intensity of 'absorption' image given in the second term in Eq. (12) (also in Eq. (5)) is based on the assumption of coherent imaging. However, Spence pointed out that the 'absorption' image is more proper to be treated as an incoherent imaging [11]. Within the resolution of ∼1 nm for biological samples, the mean absorptive potential of V_o' is the most important and interesting term. The mean absorptive potential V_o' associated with the BEPP is aperture dependent [9], and is proportional to the integral of differential elastic ($d\sigma_{el}/d\Omega$) and inelastic ($d\sigma_{el}/d\Omega$) scattering cross sections:

$$V_o'(\theta_1, \theta_2) \sim \int_{\theta_1}^{\theta_2} \left[\frac{d\sigma_{el}}{d\Omega} + \frac{d\sigma_{in}}{d\Omega} \right] 2\pi \sin\theta d\theta. \tag{13}$$

θ_1 and θ_2 are the angles related to the size of the inner (r_1) and outer (r_2) radius of the phase plate. In our phase plate, r_1 is 0.4 μm and r_2 is half the width of the cantilever (1.0 μm):

$$\theta_2 = \frac{r_2}{f} \quad \text{and} \quad \theta_1 = \frac{r_1}{f}. \tag{14}$$

Incoherent imaging of the 'absorption' contrast may be treated by a method similar to that for high-angle annular dark field (HAADF), which is different from what has been done for coherent imaging such as by the multi-slice algorithm. An intact contrast theory of BEPP to include 'absorption' and 'phase' imaging will be discussed and quantified in a later work.

Summarizing the above discussions, a central hole in a BEPP cannot be too large in order to meet the criterion of cut-off frequency for observing larger biological samples, while it cannot be too small, either, in order for sufficient amounts of unscattered electrons to pass through and be phase shifted. The size of the whole phase plate should be as small as possible in order to reduce the contribution from absorption contrast. Therefore, a BEPP design of a narrow

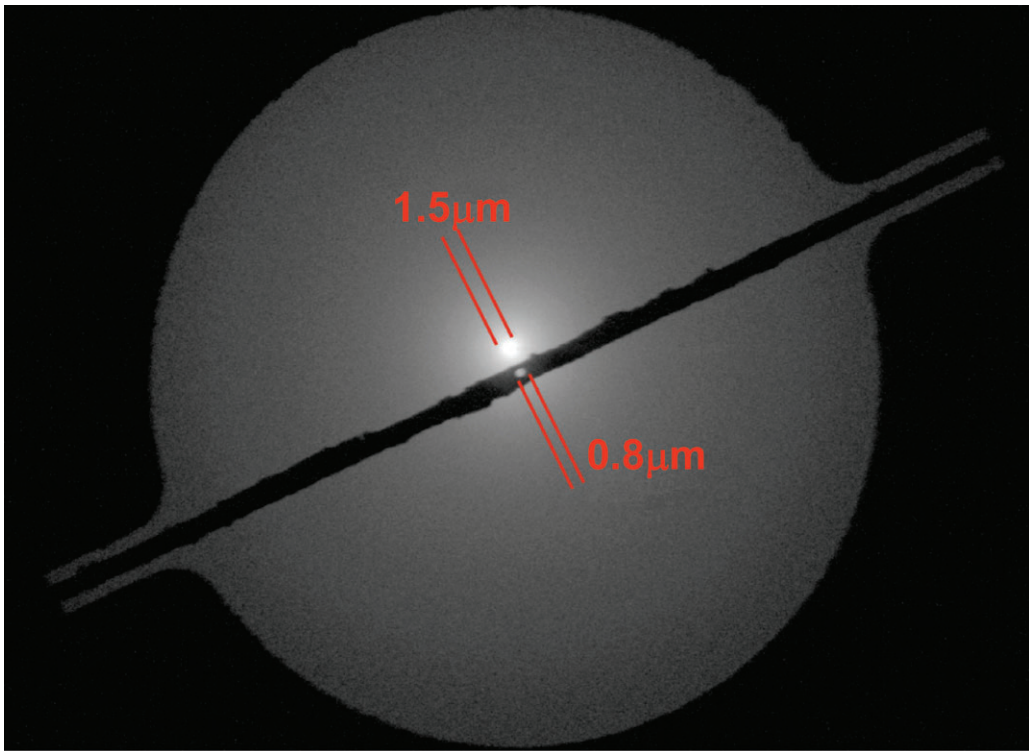

Fig. 3. The diffraction pattern taken without any sample in the beam path. The phase plate was inserted, and the central hole (0.8 μm in diameter) of the phase plate was used for calibration of the size of central diffraction spot (1.5 μm in diameter).

strip with a central hole with a proper size would be better than a BEPP designed in the shape of a ring.

Experiment

In this work, BEPPs were fabricated using nano-electro-mechanical system (NEMS) techniques on silicon substrates. As schematically shown in Fig. 1, the long cantilever has five layers: conducting, insulating, conducting, insulating and conducting, each with a thickness of ~100–200 nm. The insulating layers were constructed from Si_3N_4, through physical and chemical vapor deposition (PVD and CVD) techniques, while the conducting layers were sputter coated with Au and had an ~20 nm protecting metal layer covering the whole structure to avoid radiation damage [16]. The BEPP pattern was defined by the lithography method. A dual-beam focused ion beam system (FEI Nova 600) was used to mill the central hole on the cantilever. The detailed fabrication process of a BEPP will be reported in a separate paper.

Figure 4a shows the SEM image of a BEPP, where a long cantilever ~2.0 μm in width and 80 μm in length is suspended across an 80 μm empty hole. Figure 4b shows the central hole (~800 nm in diameter) in the middle of the cantilever, and the cross section of the hole is shown in the inset. The five-layered structure is clearly observable in the SEM image.

A TEM (JEOL 2000FX) equipped with a LaB_6 electron gun was used in this work. A preloading chamber specifically made for loading and precisely controlling the position of the BEPP was installed on this TEM system. The distribution of the electrostatic field produced by a BEPP can be found in the report by Haung *et al.* [5]. The biological samples used for this study are negatively stained ferritin corresponding to ~12 nm object size. The images were taken while the TEM was operated at 100 keV.

Results and discussion

Ferritin images

The images recorded with zero and π/2 phase shift for a negatively stained ferritin are shown in Fig. 5. All these images were recorded at zero focus to eliminate the effect of the contrast contributed from underfocusing. Figure 5a shows an image of a negatively stained ferritin recorded without insertion of the phase plate; Fig. 5b was recorded with the phase plate inserted and with zero phase shift, while Fig. 5c was taken with the phase plate in and phase shift at π/2. Some charging effects were noticed in the images when utilizing the phase plate. As shown in Fig. 5b and c, the charging effect blurs the detail of the supporting carbon film and introduces slight distortion in the diagonal direction (top/left to bottom/right). The charging effects can be reduced by increasing the thickness of the outer conducting layer of the BEPP.

Figure 5d presents the intensity profile across the ferritin. The difference between the green and the red lines represents the gain of phase contrast, while the difference

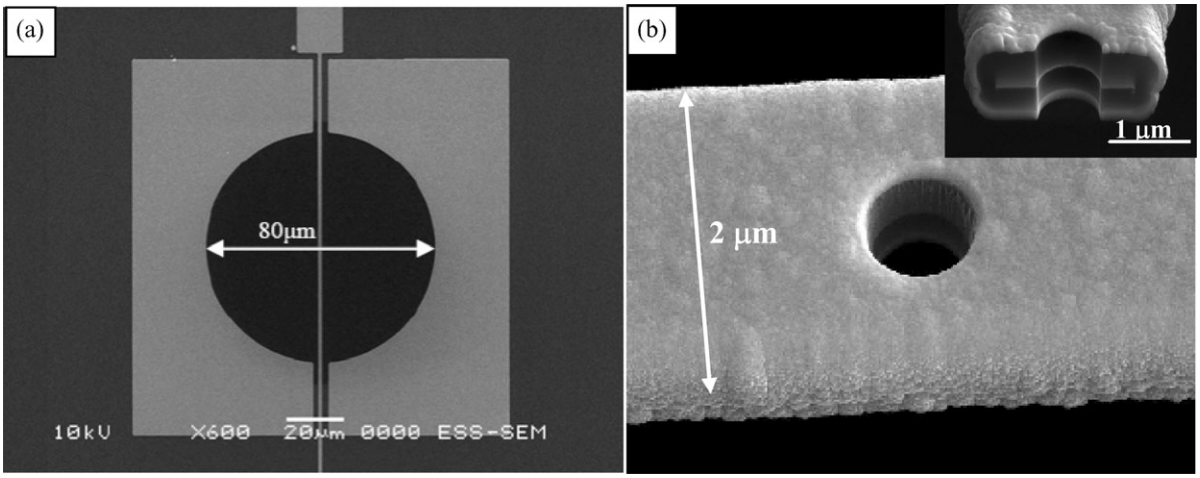

Fig. 4. SEM images of a BEPP: (a) a long cantilever ~2.0 μm in width and 80 μm in length. The cantilever is suspended across am empty circular space with a diameter of ~80 μm; (b) a central hole (~800 nm in diameter) in the middle of the cantilever. The inset shows the cross section of the hole.

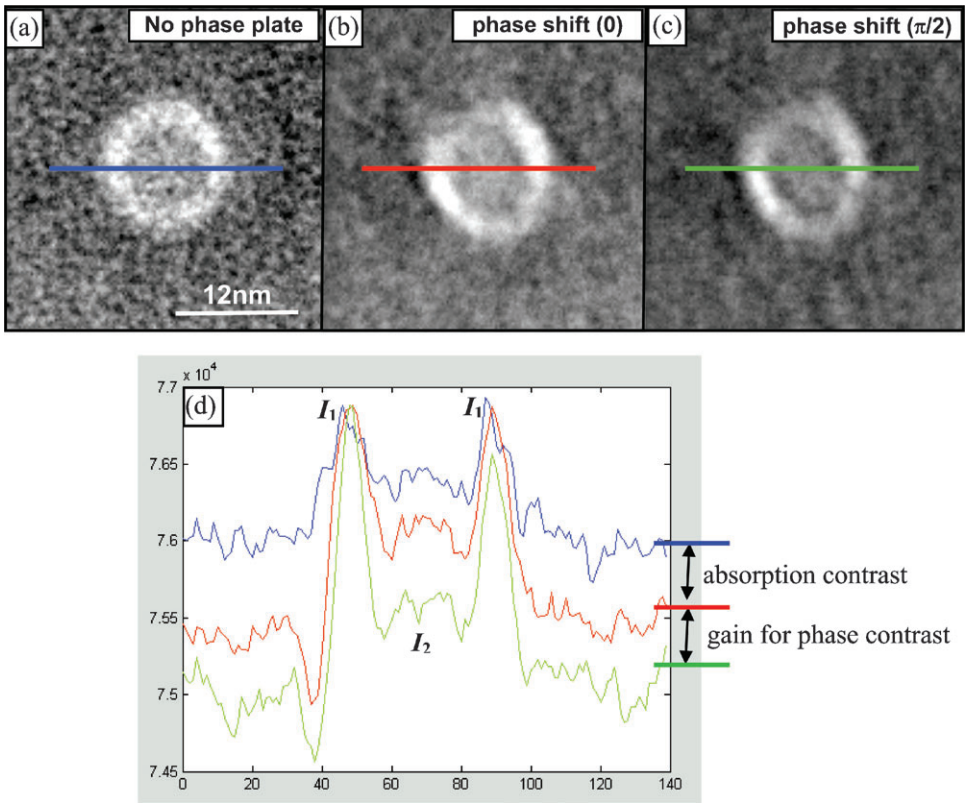

Fig. 5. Images of a negatively stained ferritin: (a) recorded without insertion of a BEPP; (b) recorded with a BEPP inserted and zero phase shift and (c) recorded with a BEPP inserted and phase shift at π/2. (d) The intensity profile across the ferritin.

between the blue and the red lines corresponds to the contribution of absorption contrast.

The phase shift produced by the Boersch phase plate is a function of the applied voltage on the electrodes of the phase plate. The phase shift was calibrated by fitting the power spectra of recorded images at a higher defocus value with calculated contrast transfer functions (CTFs). The power spectra obtained by Fourier transforms from the two images recorded at zero and π/2 phase shifts are used to demonstrate the phase shift effect from the BEPP, as shown in Fig. 6. The left portion of Fig. 6 represents the power spectrum at zero phase shift, while the right portion of the figure demonstrates the power spectrum at a phase shift of π/2; both spectra were obtained from images recorded at a

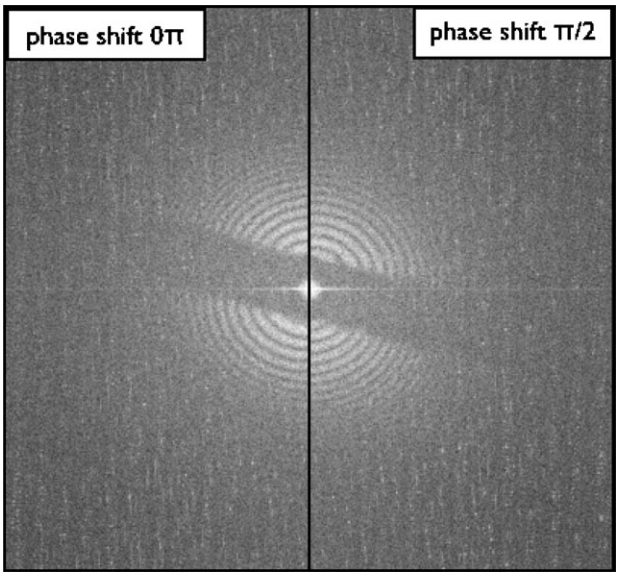

Fig. 6. The power spectra obtained from images recorded at a high defocus value, −1240 nm. The left portion represents the phase shift at 0, and the right portion represents the phase shift at π/2.

high defocus value of –1240 nm. The maxima of the squared modulus of the CTF are represented by the bright rings in the power spectrum [6]. It is clearly shown at the crossing of the two portions in Fig. 6 that the rings were shifted, indicating that the phase shift indeed occurred.

Contrast analysis

The gain of the phase contrast in ferritin images, as shown in Fig. 5, is quantified here. The image contrast can be quantified using the Rose contrast criterion [17,18] which considers the signal-to-noise ratio. The contrast, C, in the ferritin image is given by [5,18]

$$C = \frac{I_1 - I_2}{\sqrt{\sigma_1^2 + \sigma_2^2}} \tag{15}$$

where I_1 represents the averaged peak intensity in the ferritin image and I_2 represents the lowest intensity in the ferritin, as shown in Fig. 5d. σ_1 and σ_2 are the intensity variants of these two intensities, respectively. The ratio of contrast, C_R, is given by C at phase = π/2 divided by C at phase = 0, i.e.

$$C_R = \frac{(I_1 - I_2)_{\text{phase}=\pi/2}\ \left(\sigma_1^2 + \sigma_2^2\right)^{1/2}_{\text{phase}=0}}{(I_1 - I_2)_{\text{phase}=0}\ \left(\sigma_1^2 + \sigma_2^2\right)^{1/2}_{\text{phase}=\pi/2}}. \tag{16}$$

The C_R is ∼1.5 based on the calculation from Eq. (16). This value, while it is relatively low, corresponds to the practical conditions as discussed in the above sections.

In a perfect system, ∼10 times contrast enhancement is expected while utilizing a phase plate, as discussed in the theory section. In reality, however, the phase contrast is superimposed on the absorption contrast. To reveal the enhancement of the phase contrast, the gain in the phase contrast must therefore overcome the noise and the 'absorption' contrast.

As stated above, the electron beams are not ideally parallel in the present case; therefore, a BEPP is expected to block some unscatterred beams due to beam divergence. Therefore only ∼10% unscattered beam (calculated from the image shown in Fig. 3) actually passed through the central hole of the BEPP. This effect greatly reduced the efficiency of the phase contrast [i.e. the term $(I_1 - I_2)$ at phase = π/2 in Eq. (16) was reduced by this effect].

Since the unscattered beams and scattered beams are both partially blocked by the BEPP, the contribution from absorption contrast in the image was inevitable. The increase in the absorption contrast (i.e. increasing the term $(I_1 - I_2)$ at phase = 0 in Eq. (16)) further reduces the contrast enhancement. Therefore, C_R is expected to have a low value.

Conclusion

In conclusion, a TEM system with a currently available setup would provide a low efficiency in transfer of object phase to image intensity owing to the practical limitations of BEPP geometry, positioning and the illumination system used in the TEM. The theoretical and practical issues relating to the phase efficiency are discussed, and a real case of phase imaging negatively stained ferritin using a TEM with a BEPP is reported. The phase contrast was enhanced by a factor of ∼1.5 as quantified by the Rose contrast criterion. Such a low gain of phase contrast is consistent with our expectations from the present TEM/BEPP system.

An effective phase TEM for biological imaging utilizing a BEPP, therefore, should consist of the following components:

(i) A uniform/parallel illumination, in order to make the central diffracted spot sufficiently small. This can be achieved by modifying the TEM illuminating and lense system.
(ii) A reliable electrostatic phase plate, with a proper size of the central hole, which is small enough (<1 μm, or depending on the focal length of the TEM) for observing larger biological samples and large enough for sufficient numbers of unscattered electrons to pass through. The overall dimension of the phase plate (the cantilever) should be as small as possible to limit the contribution from absorption contrast.
(iii) A precisely controlled phase plate positioning system, which can position the phase plate at the exact back focal plane without tilting.

Funding

This work was partly supported by the National Science Council, and the thematic project from Academia Sinica of Taiwan.

Acknowledgements

Technical supports from NanoCore, the Core Facilities for Nanoscience and Nanotechnology at Academia Sinica, are acknowledged.

References

1 Danev R, and Nagayama K (2001) Transmission electron microscopy with Zernike phase plate. *Ultramicroscopy* **88**: 243–252.

2 Danev R, and Nagayama K (2008) Single particle analysis based on Zernike phase contrast transmission electron microscopy. *J. Struct. Biol.* **161**: 211–218.

3 Nagayama K (2008) Development of phase plates for electron microscopes and their biological application. *Eur. Biophys. J.* **37**: 345–358.

4 Matsumoto T, and Tonomura A (1996) The phase constancy of electro waves traveling through Boersch's electrostatic phase plate. *Ultramicroscopy* **63**: 5–10.

5 Huang S H, Wang W J, Chang C S, Hwu Y K, Tseng F G, Kai J J, and Chen F R (2006) The fabrication and application of Zernike electrostatic phase plate. *J. Electron Microsc.* **55**: 273–280.

6 Schultheiβ K, Pérez-Willard F, Barton B, Gerthsen D, and Schröder R R (2006) Fabrication of a Boersch phase plate for phase contrast imaging in a transmission electron microscope. *Rev. Sci. Instrum.***77**: 33701.

7 Cambie R, Downing K H, Typke D, Glaeser R M, and Jin J (2007) Design of a microfabricated, two-electrode phase-contrast element suitable for electron microscopy. *Ultramicroscopy* **107**: 329–339.

8 Malac M, Beleggia M, Egerton R, and Zhu Y (2008) Imaging of radiation-sensitive samples in transmission electron microscopes equipped with Zernike phase plates. *Ultramicroscopy* **108**: 126–140.

9 Chen K F, Chang C S, Shiue J, Hwu Y K, Chang W H., Kai J J, and Chen F R (2008) Study of mean absorptive potential using Lenz model: toward quantification of phase contrast from an electrostatic phase plate. *Micron* **39**: 749–756.

10 Majorovits E, Barton B, Schultheiss K, Pérez-Willard F, Gerthsen D, and Schröder R R (2007) Optimizing phase contrast in transmission electron microscopy with an electrostatic (Boersch) phase plate. *Ultramicroscopy* **107**: 213–226.

11 Spence J C H (2003) *Experimental High Resolution Transmission Electron Microscopy*, 3rd edn (Oxford University Press, New York).

12 Yoshioka H (1957) Effect of inelastic waves on electron diffraction. *J. Phys. Soc. Japan* **12**: 618–628.

13 Hashimoto H, Howie A, and Whelan M J (1962) Anomalous electron absorption effects in metal foil-theory and comparison with experiment. *Proc. R. Soc. A* **269**: 80.

14 Humphreys C J, and Hirsch P B (1968) Absorption parameters in electron diffraction theory. *Phil. Mag.* **18**(1968): 115–122.

15 Bird D M, and King Q A (1990) Absorptive form factors for high-energy electron diffraction. *Acta Cryst.* **A46**: 202–208.

16 Egerton R F, Li P, and Malac M (2004) Radiation damage in the TEM and SEM. *Micron* **35**: 399–409.

17 Rose A (1948) Television pickup tubes and the problem of vision. In: Marton L (ed.), *Advances in Electronics and Electron Physics*, pp 131–166 (Academic, New York).

18 Cunningham I A, and Shaw R (1999) Signal-to-noise optimization of medical imaging systems. *J. Opt. Soc. Am. A* **16**: 621–632.